Available online at www.sciencedirect.com
SCIENCE DIRECT®
International Journal of Heat and Mass Transfer 48 (2005) 2759–2770
International Journal of HEAT and MASS TRANSFER
www.elsevier.com/locate/ijhmt

Method to improve geometry for heat transfer enhancement in PCM composite heat sinks

R. Akhilesh, Arunn Narasimhan *, C. Balaji

Heat Transfer and Thermal Power Laboratory, Department of Mechanical Engineering, Indian Institute of Technology Madras, Chennai 600 036, India

Received 29 September 2004; received in revised form 21 December 2004
Available online 7 April 2005

Abstract

Use of composite heat sinks (CHS), constructed using a vertical array of 'fins' (or elemental composite heat sink, ECHS), made of large latent heat capacity phase change materials (PCM) and highly conductive base material (BM) is a much sought cooling method for portable electronic devices, which are to be kept below a set point temperature (SPT). This paper presents a thermal design procedure for proper sizing of such CHS, for maximizing the energy storage and the time of operation until all of the latent heat storage is exhausted.

For a given range of heat flux, q'', and height, A, of the CHS, using a scaling analysis of the governing two dimensional unsteady energy equations, a relation between the critical dimension for the ECHS and the amount of PCM used (ϕ) is determined. For a ϕ, when the dimensions of the ECHS are less than this critical dimension, all of the PCM completely melts when the CHS reaches the SPT. The results are further validated using appropriate numerical method solutions. A proposed correlation for chosen material properties yields predictions of the critical dimensions within 10% average deviation. However, the thermal design procedure detailed in this paper is valid, in general, for similar finned-CHS configurations, composed of any high latent heat storage PCM and high conductive BM combination.

Keywords: Heat transfer enhancement; Scale analysis; Phase change material; Composite heat sink; Electronics cooling

1. Introduction

Thermal management is seen as one of the most significant bottlenecks in the development of faster microprocessors used in portable electronic devices [1]. As the reliability of the electronic components is a very strong function of temperature [2], their cooling (thermal) design should successfully address the issue of keeping the working temperature of such devices below a critical value, characteristic of individual configurations.

Use of phase change materials (PCM) based heat sinks are prevalent in the recent decade [2–6] in cooling portable devices such as palm pilots, cellular phones and personal digital assistants, as these devices seldom are used for more than a few hours continuously at peak load and their 'idle' time is typically long enough to solidify the molten PCM for reuse. PCMs are also

* Corresponding author. Tel.: +91 44 22578528; fax: +91 44 22578501.
E-mail addresses: arunn@iitm.ac.in (A. Narasimhan), balaji@iitm.ac.in (C. Balaji).

0017-9310/$ - see front matter © 2005 Elsevier Ltd. All rights reserved.
doi:10.1016/j.ijheatmasstransfer.2005.01.032

Nomenclature

A	height of the CHS, m, Fig. 1
b	melt-front distance from x axis at a given time t, m, Fig. 2
B	width of PCM in ECHS, m, Fig. 2, Eq. (10)
BM	base material, Table 1
c	specific heat, kJ/kg K
CHS	composite heat sink
D	overall width of CHS, m, Fig. 1
E	energy per unit area, J/m^2
ECHS	elemental composite heat sink
E_R	enhancement ratio, Eqs. (9) and (27)
F	number of fins (1 fin = 2 × ECHS) per unit length, Eq. (12)
k	thermal conductivity, W/m K
L	latent heat of PCM, kJ/kg
N	number of fins (1 fin = 2 × ECHS), Eq. (11)
PCM	phase change material, Table 1
q''	heat flux, W/m^2
SPT	set point temperature criterion, Eq. (1)
Ste	Stefan Number, Eq. (21)
t	time, s
T	temperature, °C
x, y	Cartesian coordinates

Greek symbols

γ	heat capacity ratio, Eq. (22)
Γ	net energy inside ECHS calculated numerically/$[q''(B + d)t]$
δ	width of BM in ECHS, m, Fig. 2
ϕ	ratio of volume of PCM to total volume of CHS
ρ	density, kg/m^3
σ	standard deviation, Eq. (6)
σ_{REL}	relative average deviation, Eq. (26)
τ	time taken by CHS to reach SPT, Eq. (20), s
ζ	length scale factor in correlation Eq. (25)

Subscripts

BM	base material (here, aluminum, Table 1)
c	critical value
i	initial value
I	isothermal case, Eq. (7)
M	melting point
MAX	maximum
NI	non-isothermal case, Eq. (8)
P, PCM	phase change material
SET	set point

used in heat sinks cooling devices where heat dissipation is expected to vary with time [4]. The objective of PCM usage in such instances is to keep the temperature of the electronic device below a critical temperature—usually the junction temperature of silicon, which is 90 °C [5,6].

However, PCMs (such as paraffin, Eicosane) are characterized by very low thermal conductivity [7,8] and so directly dissipating the heat generated by the electronics into a column of PCM from the top results in the electronic components reaching unsafe temperatures (above their junction temperatures) even before a significant quantity of the PCM melts, not fulfilling the purpose of exhausting the latent heat storage for cooling. In the light of this, active research is being done [2,3,7] in designing a composite heat sink (CHS), involving PCM and a base material (BM) to 'bring' the heat into the PCM—one common CHS design being that of BM fins protruding into a reservoir of PCM [2,9–11]. Sasaguchi and Kusano [10] have performed excellent investigations using quasi-steady models for finned PCM-CHS by treating them as porous media and a similar quasi steady model analysis for finned PCM-CHS geometry not very different from the one considered in this paper has been proposed by Krishnan et al. [11] for a hybrid heat–sink. However, they have not considered the sizing of the geometry of the CHS for better performance. Natural convection inside the molten PCM then becomes important [12,13] which could alter the time of operation of the CHS.

When receiving a constant rate of energy from the electronics (constant heat flux crossing a boundary), an 'efficient' CHS could be one that completely exhausts its PCM latent heat storage (maximum energy is stored) in the longest time (thus increasing the time of operation of the electronics), without allowing the electronics to reach unsafe temperatures. Hence, it is essential that the CHS is designed with a judicious combination of high conductivity BM (carrying away the heat, quickly from the electronics) with the PCM (storing the heat as latent heat). The cost of the CHS is directly related to the quantity of PCM and BM used and their manufacture into 'fin' shapes (Fig. 1a). Hence, this situation translates to the question of how, for a given quantity of PCM, one can choose the 'best' dimensions of BM and PCM within the CHS, for better performance. The objective of this paper is to delineate a design procedure that would answer the above question for a set of CHS design constraints (Table 1).

2. Composite heat sink

Fig. 1 illustrates, schematically, the CHS studied in this paper. The CHS is insulated on all sides but for the top wall through which the heat dissipated from

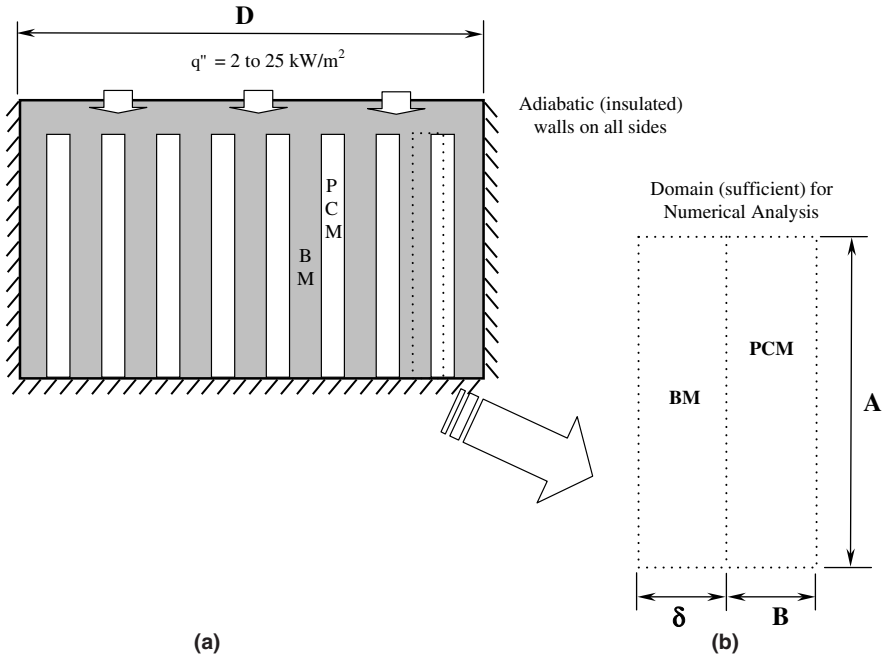

Fig. 1. (a) Schematic of the CHS design and (b) domain sufficient for numerical analysis.

Table 1
Parameters and material properties used in the study

Parameters	Symbol	Values/range used in simulation
PCM porosity	ϕ	0.0–0.8
SPT	T_{SET} (K)	360
Height, Fig. 1	A (m)	0.03, 0.05, 0.07
Heat Flux	q''(kW m^{-2})	2, 7 and 25
BM properties [20]	ρ (kg m^{-3})	2702
	k (W m^{-1} K^{-1})	237
	c (kJ kg^{-1} K^{-1})	0.9
PCM properties [22]	ρ (kg m^{-3})	800
	k (W m^{-1} K^{-1})	0.24
	c (kJ kg^{-1} K^{-1})	2.5
	L (kJ kg^{-1})	266
	T_M (K)	310

the electronic components enter. The insulated condition is in line with the proposed heat sink design here for cooling portable devices, which incur only minimal natural convective losses to the surrounding (radiative losses are safely neglected for the maximum temperatures involved). Further, the assumption of insulated walls provides a conservative design procedure even when the losses become significant.

A thin layer of BM sandwiched between the BM/PCM fin array and the top wall (see Fig. 1), ensures that the PCM is not in direct thermal contact with the electronic components on the top wall. One would then expect—because of the high k_{BM}—the heat crossing the top wall could traverse the high conducting BM path and melt the PCM more from the sides. It can be observed that the heat could as well enter the PCM from the top and a commonplace argument would support this design. However, even for the nominal heat fluxes encountered in these designs ($\sim$2000 W/m^2, [7]) the simple bluff shape of the PCM array would immediately induce hot spots above them. One simple way to circumvent this problem is to provide a layer of base material between the fins and the electronic equipment. The thickness of this BM layer should be such that hot spots and large temperature gradients are avoided across the layer. Similar heat spreader layers have been provided in [11,14] and their effect has been neglected in the respective analyses as typically one would expect an insubstantial temperature gradient of 1–2 K across the BM layer. Deeming this heat spreader to be in place, the domain shown in Fig. 1b is sufficient for the numerical analysis. Natural convection is neglected in the analysis, an approach common while investigating such problems [5,9,11,15].

Defining a *set point temperature criterion* (SPT) as the condition when the maximum temperature of the domain is equal to the set point in temperature, i.e.,

$$T_{MAX} = T_{SET} \tag{1}$$

the goal would be to provide suitable design dimensions (δ and B) for the ECHS (Fig. 1b) for a given ϕ of PCM, which will ensure the longest possible time of CHS operation for a stated SPT.

3. Modeling procedure and numerical method

Fig. 2 shows all of the boundary conditions involved in the numerical simulation procedure. Neglecting the temperature gradients in the y direction (assuming a thin fin after [9]), the governing equation in the BM domain is

$$k_{\mathrm{BM}}\delta\frac{\partial^2 T_{\mathrm{BM}}}{\partial x^2}+k_{\mathrm{P}}\frac{\partial T_{\mathrm{P}}}{\partial y}\bigg|_{y=0}=(\rho c)_{\mathrm{BM}}\delta\frac{\partial T_{\mathrm{BM}}}{\partial t} \tag{2}$$

The first and the third terms of Eq. (2) are the familiar terms of one-dimensional transient conduction inside the BM domain while the second term indicates the heat absorbed by the PCM, which is evaluated as a differential flux at the interface. In addition, a temperature parity term is enforced at $y = 0$ as

$$T_{\mathrm{P}}(x,0,t)=T_{\mathrm{BM}}(x,t) \tag{3}$$

assuming zero contact resistance between the BM and PCM domain. The PCM domain is considered to be a two dimensional area governed by

$$k_{\mathrm{P}}\left[\frac{\partial^2 T_{\mathrm{P}}}{\partial x^2}+\frac{\partial^2 T_{\mathrm{P}}}{\partial y^2}\right]=(\rho c)_{\mathrm{P}}\frac{\partial T_{\mathrm{P}}}{\partial t} \tag{4a}$$

As shown in Fig. 2, the PCM domain is insulated on three sides and heated on one side by a BM fin. The one dimensional fin Eq. (2) and the two dimensional Eq. (4) are coupled through the interface condition set in Eq. (3), which controls the second term in Eq. (2). The PCM latent heat term does not appear explicitly in Eq. (4). The differences in the incoming and outgoing heat fluxes for a control volume (around a grid point) is the energy inventory going into melting the PCM vol-

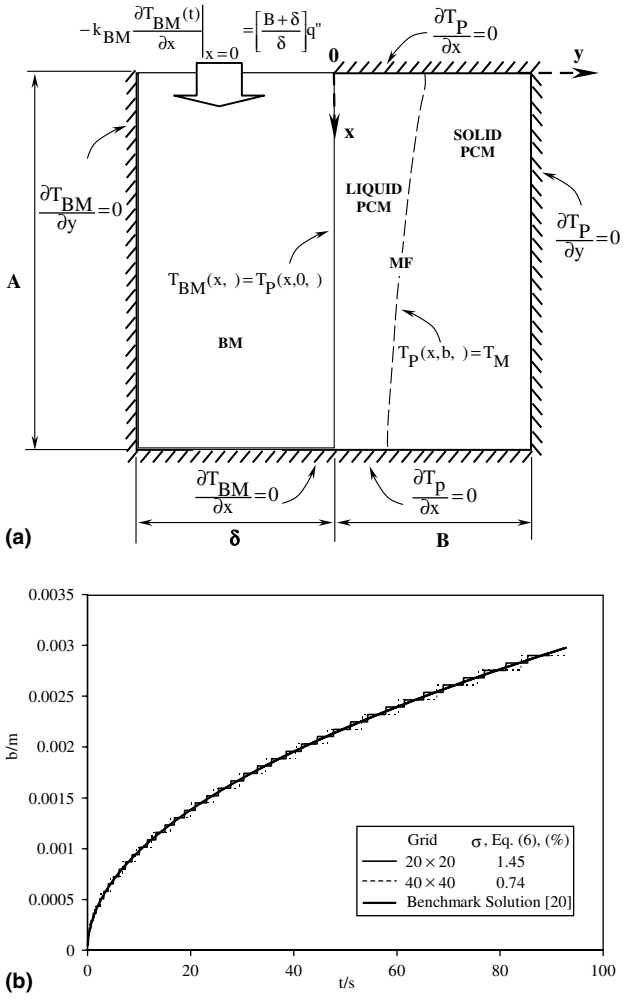

Fig. 2. (a) ECHS domain and boundary conditions used for the numerical simulations. (b) Melt front position b (m) versus time t (s): benchmark validation of the melting solver.

ume about that control volume (grid point). The solid–liquid interface (melting front, b) is written as

$$T_P(x, y_b, t) = T_M \tag{4b}$$

While using numerical methods to solve Eq. (4a), the PCM melt-front is tracked by using this metering of the energy interactions of the grid point (control volume) that satisfies Eq. (4b) by changing phase in the PCM domain. This simple formulation is similar to the enthalpy formulation for describing the melt-front evolution employed in similar numerical simulations [16,18]. The deployment of an adiabatic boundary condition $\partial T_P/\partial x = 0$ at the top wall of the PCM domain assumes the streamlining mentioned in the previous section. Since the ECHS in Fig. 2 repeats to fill the CHS space in Fig. 1a, following [11,17], adiabatic conditions for the ECHS is employed on the side and bottom walls as well. In essence, the ECHS in Fig. 2 is a one dimensional BM fin that loses heat to a melting-conductive PCM surrounding.

Eqs. (2) and (4) are solved by numerical methods for the parameters and material properties listed in Table 1 with the initial condition of

$$T_{BM}(x, y) = T_P(x, y) = T_i \quad \text{at } t = 0 \tag{5}$$

and for the boundary conditions discussed (and listed in Fig. 2). The calculations are stopped when the maximum temperature of the ECHS domain satisfies SPT, Eq. (1). Aluminum (for BM) is chosen for its high conductivity and the PCM used is *n-Eicosane* (Table 1), the standard paraffin used in similar kind of electronics cooling applications [3] because of its high latent heat of fusion. Further, its melting point (~310 K) also strategically falls between the ambient temperature and the usual maximum allowable temperature (T_{SET}) values for electronic components [7,8].

The numerical method involves a discrete melting front formulation, adopting a finite difference method using second order accurate central differencing schemes. An implicit scheme in the BM domain and an alternating direction implicit (ADI) scheme in the PCM domain, both unconditionally stable schemes [19] were made use of to solve Eqs. (2) and (4) respectively. The solution was obtained using a 40 element grid in the BM and a 40×40 rectangular grid in PCM, which were tested for grid as well as time step independence. As can be seen in Table 2, the 20×20 and 40×40 grids predict the ECHS numerical versus actual energy balance result (Γ) within 1%, and so the result is grid-size independent. The results in Table 2 also show the time-step independence at a Δt of 0.0025 s for a 40×40 grid. Further, the melting solver is validated in the PCM domain of $A = 0.05$ m and $B = 0.003$ m, by solving Eq. (2) with a constant temperature boundary condition on the aluminum fin (left wall of the PCM domain in Fig. 2a) and comparing the numerical results

Table 2
Results showing grid and time-step independence of the numerical solutions

$q'' = 25$ kW/m^2; $\phi = 0.5$ ($\delta = B = 0.03$ m); $A = 0.05$ m				
20×20 grid points (PCM)			40×40 grid points (PCM)	
20 grid points (BM)			40 grid points (BM)	
Δt (s)	τ (s)	Γ (%)	τ (s)	Γ (%)
0.10	421.8	109.3	–	–
0.05	442.0	103.9	–	–
0.01	453.9	101.0	446.4	102.9
0.005	455.2	100.6	452.5	101.4
0.0025	455.8	100.5	455.1	100.8
0.001	–	–	456.7	100.4

for 20×20 and 40×40 grid in Fig. 2b, with the analytical solution (Stefan problem) presented in [20]. As explained in [21], this is a standard benchmarking procedure for phase change solvers. The standard deviation of the numerically calculated melt-front position (b) from the analytical solution in Fig. 2b is determined by

$$\sigma = \left(\frac{1}{M} \sum_{1}^{M} (b_{num} - b_{anal})^2 \right)^{1/2} \tag{6}$$

over all the M time steps. The σ for a 20×20 grid is 1.45 and for a 40×40 grid is 0.74% of B respectively. Based on the above results, a 40×40 grid in the PCM domain with a time step of 0.0025 sec is used for all the subsequent calculations.

4. ECHS performance: isothermal upper-bound

Given the basic design and constraints proposed in Figs. 1 and 2, the theoretical maximum energy storage inside the CHS is when the entire CHS is at a constant temperature at all times during operation (the CHS temperature is spatially invariant but unsteady until the SPT is met). This is referred to as the isothermal upper-bound energy E_I (J/m^2), expressed using a simple "lumped" energy balance in the CHS as

$$E_I = A\left[((1-\phi)\rho c(T_{SET} - T_i))_{BM} + (\phi \rho c_P (T_{SET} - T_i) + \phi \rho L)_{PCM}\right] \tag{7}$$

The first two terms on the RHS are the sensible heat terms of the BM and PCM respectively (the PCM is assumed to possess identical thermo-physical properties in both the solid and liquid phases) while the third term accounts for the energy stored in the latent heat of melting. Eq. (7) is valid even for the extreme limits, i.e., a CHS filled with BM ($\phi = 0$) or PCM ($\phi = 1$).

Even if we consider the CHS is to be composed only of BM, when it receives heat in actual situations

of operation, the temperature gradients even at the elemental level (ECHS) are inevitable. Hence the energy stored in the non-isothermal CHS (actual case of operation) is always lesser than the, thermodynamically reversible, theoretical maximum (E_I from Eq. (7), for $\phi = 0$). This ''non-isothermal'' energy stored in the CHS completely filled with BM ($\phi = 0$) can be obtained analytically by solving the transient conduction equation with adiabatic boundary conditions on all sides except the heated top wall (Fig. 1). The same result is obtained using a finite difference scheme for solving the unsteady conduction equation. Using the numerical results obtained when the SPT is reached for 35 sample-data (obtained for several combinations of A and q''), the maximum energy stored in the non-isothermal CHS composed only of BM can then be written as

$$E_{NI}|_{\phi=0} = E_I|_{\phi=0} - q''(x_1A^2 + x_2A + x_3) \tag{8}$$

for $0.03 \leqslant A \leqslant 0.07$, with $x_1 = 3.482\ \mathrm{m}^{-2}\,\mathrm{s}$, $x_2 = -0.6829\ \mathrm{m}^{-1}\,\mathrm{s}$ and $x_3 = 0.0341\ \mathrm{s}$. Using Eq. (8), we can define a non-dimensional enhancement factor E_R as

$$E_R = \frac{E_{NI}(\phi)}{E_{NI}|_{\phi=0}} \tag{9}$$

where $E_{NI}(\phi)$ is the energy per unit area that could be stored in the CHS containing both PCM and BM. This figure of merit compares the CHS (with PCM) with a heat sink made only of BM.

5. Results for arbitrary ECHS dimensions

For a fixed SPT, at a given q'' and A, to employ the ECHS design in Fig. 1b for each ϕ, we require the value of B, which can be obtained (using the definition of ϕ) as

$$B = \frac{\delta\phi}{1-\phi}, \tag{10}$$

provided the value of δ is known a priori. For a given A, the total number of ECHS (Fig. 1b) fins of dimension δ and B (which are related to ϕ by Eq. (10)) to fill the entire CHS of Fig. 1a is

$$N = \frac{D}{2(B+\delta)} \tag{11}$$

which, by eliminating B between Eq. (11) and the definition of ϕ ($=B/B+\delta$), could be expressed as the ECHS fins per unit length of the CHS as

$$F = \frac{N}{D} = \frac{(1-\phi)}{2\delta}. \tag{12}$$

Eq. (12) shows that F depends only on ϕ and δ, the two design parameters required to determine the size of the ECHS. However, an arbitrary choice of δ for the ECHS (which for any chosen ϕ, would certainly define a B, Eq. (10), for the ECHS) could lead to a poorly performing ECHS upon reaching the SPT, because of incomplete melting, as shown in Fig. 3. In general, as the temperature gradients approach zero, the isotherms become normal to the insulated top walls, as can be seen in the figure. The melt-front (MF) in the PCM domain is not parallel to the BM fin, but is inclined away from the reference vertical 'x' axis. The MF extends deeper into the PCM near the heated top wall of the BM fin. This inclination is due to the temperature profile in the BM fin, as can be seen in Fig. 3a.

The above situation (Fig. 3) of arbitrary ECHS dimensions (fixing any δ and therefore B, for a given ϕ) leading to some un-melted PCM remaining when SPT is reached, does not result in a better performing CHS. Hence, the first task is to determine a δ that completely melts all of the PCM for each chosen value of ϕ, *exactly when* the SPT is reached.

6. Finding the best δ for a given ϕ

For a chosen ϕ, in a limiting sense, the CHS (Fig. 1) could be constructed with only one ECHS (Fig. 1b) with δ and B chosen such that their relationship with ϕ, Eq. (10), is satisfied. In this case, δ and B take maximum possible values, but the CHS has *least* heat transfer surface area between the BM and PCM. Obviously, the other limiting case of a CHS (Fig. 1a) with an infinite number of ECHS (Fig. 1b) having minimum values for and B (δ and $B \to 0$, so, $N \to \infty$) may be impractical. To completely melt the PCM when the SPT is reached, a 'critical' dimension for and B that falls between the above two limits is required, which provides large enough heat transfer area between BM and PCM inside the ECHS to ensure complete PCM melting. For a given quantity of PCM (ϕ) and a fixed q'' from the top wall, as the CHS is made of finite numbers of ECHS, the procedure to find the ECHS critical dimensions is independent of D, the overall dimension of the CHS (Fig. 1a).

Taking the above discussion as a guideline, an automated binary search for the ϕ and q'' of Fig. 3 was performed to locate the satisfactory δ and B for the ECHS, at which all of the PCM in Fig. 3 completely melts. To assist in this search, for each trial run, the percentage of melted PCM (ε) at the time when SPT is reached is calculated. A value of $\delta = \delta_c$ (and from Eq. (10), $B = B_c$) which assures a value of ε between 99% and 100% on reaching SPT is sought. For the q'' and ϕ used in Fig. 3, Fig. 4 is a plot of the number of ECHS fins per unit length F, Eq. (12), versus τ, the time taken by the ECHS to reach SPT for the corresponding δ value. From the figure it is clear that the arbitrary δ value chosen in Fig. 3 (the corresponding $F = 50$, marked by a circle in Fig. 4) does not yield the best time of operation when the SPT is reached. The critical δ_c value for which

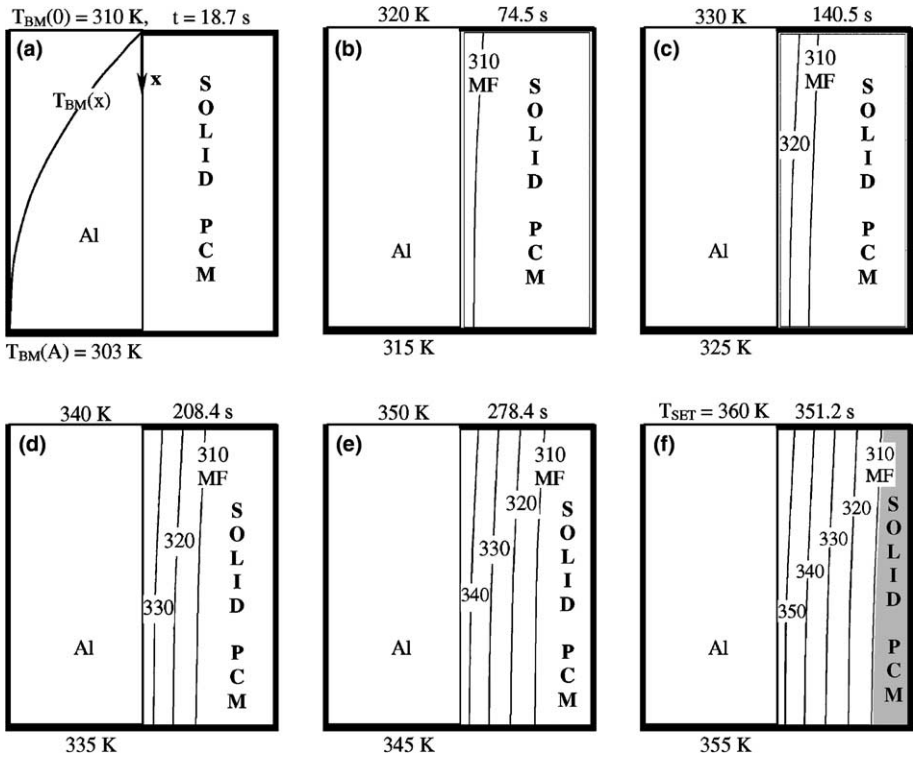

Fig. 3. Melt front evolution in time (a–f) until the SPT is reached, for arbitrary ECHS dimensions ($\delta = B = 0.005$ m) for $\phi = 0.5$, $q'' = 25$ kW/m^2, $A = 0.05$ m.

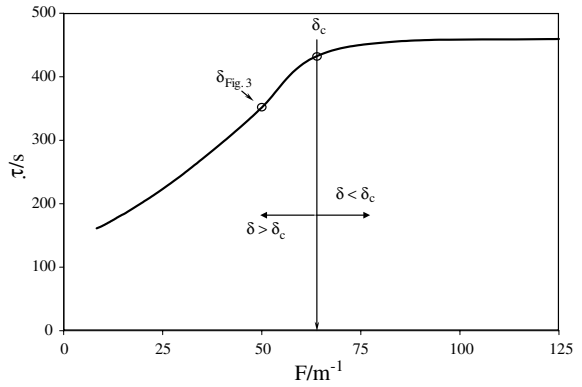

Fig. 4. F versus ϕ: Finding best δ dimensions for a ϕ ($\phi = 0.5$, $q'' = 25\,000$ W/m^2).

complete melting takes place when the SPT is reached is actually smaller, thus allowing more number of fins per unit length (F increases from 50 to 65) and hence more heat transfer area between BM and PCM domains in each of the ECHS. This improves the operation time of the ECHS (and hence, the CHS) to about 425 s. Decreasing δ below the δ_c (located at the elbow of the graph) value, which leads to more number of fins (F) nevertheless, increases the time of operation (and energy stored) only marginally as the PCM has already been fully melted.

For values of ϕ, q'' and A used in Fig. 3, the above critical dimensions of the ECHS, as discussed above, ensure that all of the PCM latent heat is utilized in Eq. (7), which can be witnessed in the temperature contours of Fig. 5. Fig. 5a shows the temperature contours at the time when the case depicted in Fig. 3 reaches SPT (Fig. 3f). Fig. 5b shows the temperature contours when the critical dimensioned ECHS reaches the SPT (at a longer time). The contours are not mildly inclined as in the previous cases (Fig. 3), but are curved—showing the heat transfer in the PCM is indeed two dimensional. A 77 s increase is witnessed in the time of operation of the ECHS (thereby, the CHS) for the present case, before the SPT is reached. Comparing with the earlier case (Fig. 3), for identical values of ϕ, q'' and A, this clearly portrays the effect of improved ECHS geometry (δ_c and B_c) in bettering the performance of the CHS.

7. Best B and δ prediction: scale analysis

For fixed material constraints (BM and PCM properties in Table 1) and CHS parameters (q'' and A), scale

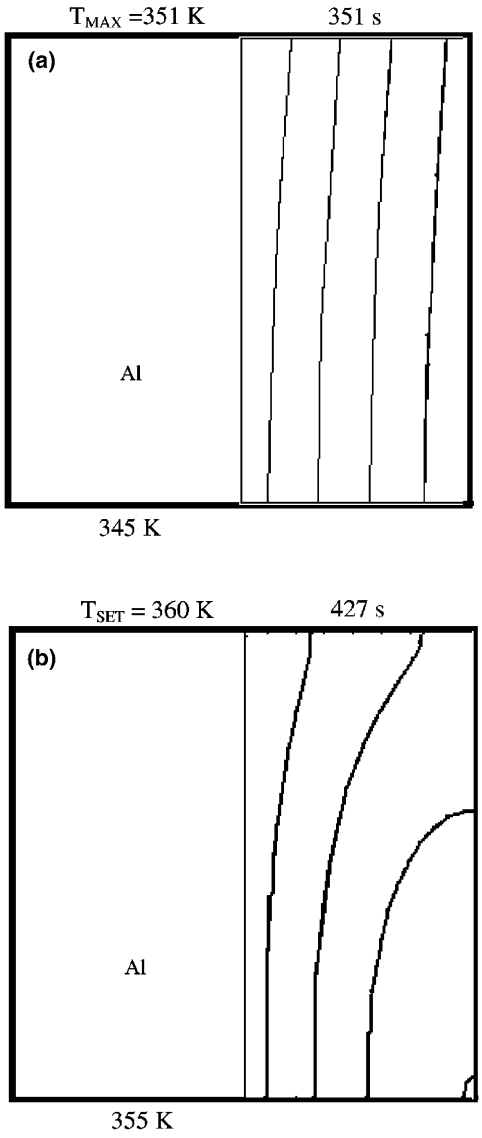

Fig. 5. Improvement in the time of operation of the ECHS of Fig. 3 ($\phi = 0.5$, $q'' = 25\ \mathrm{kW/m^2}$, $A = 0.05$ m) with critical dimensions ($\delta = B = 0.003$ m). Melt front for best ECHS (a) $t = 351.0$ s, the time when ECHS of Fig. 3 reached (b) $t = 427.76$ s, time when SPT is reached.

analysis can be used to estimate the δ_c and B_c of the ECHS for any ϕ, ensuring complete melting *when* SPT is reached. In performing the scale analysis inside the ECHS (Fig. 2), the BM domain is treated as a "lumped" system owing to its high thermal conductivity ($k_{BM} \gg k_{PCM}$). A lumped BM temperature value (T_{BM}) renders the conduction problem in the PCM domain one dimensional, since the top and the bottom ends of the PCM domain are insulated (see Figs. 1 and 2).

Following the procedure listed in [20] for the energy balance inside the control volume around the melt-front progressing in time, the phase change is governed by

$$\frac{\partial b}{\partial t}\left(\frac{\rho L}{k}\right)_{\mathrm{PCM}} = \left.\frac{\partial T}{\partial y}\right|_{\mathrm{l,b}} - \left.\frac{\partial T}{\partial y}\right|_{\mathrm{s,b}} \tag{13}$$

where subscripts 'l' and 's' are for liquid side and solid side of the PCM control volume. Treating the solid, un-melted, PCM as isothermal, we can write

$$\left.\frac{\partial T}{\partial y}\right|_{\mathrm{s,b}} = 0 \tag{14}$$

as the temperature gradient scale for the solid PCM. The temperature of the BM domain varies from T_i to T_{SET}, Taking $T_i = T_M$, for $0 < \phi < 1$, the melting temperature of the PCM, the scale for the lumped T_{BM} can be written as

$$T_{\mathrm{BM}} \sim \frac{T_{\mathrm{SET}} + T_{\mathrm{M}}}{2} \tag{15}$$

It is to be kept in mind that the scaling conclusion drawn in Eq. (15) is not valid when the ECHS (therefore the CHS) is composed either only of BM ($\phi = 0$) or only of PCM ($\phi = 1$). For a linear temperature variation inside the molten PCM (not a bad assumption for $B \ll A$ inside the ECHS) using Eq. (15), we can write

$$\left.\frac{\partial T}{\partial y}\right|_{\mathrm{l,b}} = \frac{T_{\mathrm{BM}} - T_{\mathrm{M}}}{b} \tag{16}$$

Using Eqs. (14)–(16), the melt-front velocity, Eq. (13), can be scaled as

$$\frac{\mathrm{d}b}{\mathrm{d}t}\left(\frac{\rho L}{k}\right)_{\mathrm{PCM}} \sim \frac{(T_{\mathrm{BM}} - T_{\mathrm{M}})}{b} \tag{17}$$

which upon integrating for the entire melt process with the condition that complete melting is reached ($b = B$) when the SPT is reached ($t = \tau$) yields a scale for the maximum PCM thickness B in the ECHS domain as,

$$B \sim \sqrt{\frac{2k_{\mathrm{PCM}}(T_{\mathrm{BM}} - T_{\mathrm{M}})\tau}{\rho_{\mathrm{PCM}} L}}, \tag{18}$$

a result consistent with the analysis in [20], done for a semi-infinite domain of PCM. Since the above scaling is done for the case of complete melting *when* the SPT is reached, the value of B obtained from Eq. (18) is the best value for the ECHS that is sought and τ is the time of operation.

The best time of operation τ, the only unknown in Eq. (18), can be estimated by altering the isothermal energy balance in the ECHS, Eq. (7), suitably for complete melting when the SPT is reached. By invoking the linear temperature profile assumption in the PCM and using the definition of T_{BM}, Eq. (15), the sensible heat term of the PCM in the isothermal ECHS energy balance, Eq. (7), can be re-written as

$$\phi(\rho c)_{\mathrm{PCM}}(T_{\mathrm{BM}}-T_{\mathrm{M}})=\phi(\rho c)_{\mathrm{PCM}}\left[\frac{T_{\mathrm{SET}}+T_{\mathrm{M}}}{2}-T_{\mathrm{M}}\right]=\phi(\rho c)_{\mathrm{PCM}}\frac{(T_{\mathrm{SET}}-T_{\mathrm{M}})}{2} \tag{19}$$

Hence τ, the time scale for complete melting when SPT is reached is obtained as

$$\tau\sim\frac{A}{q''}\left[(\rho c)_{\mathrm{BM}}(T_{\mathrm{SET}}-T_{\mathrm{M}})(1-\phi)+\rho_{\mathrm{PCM}}\left(L+c_{\mathrm{PCM}}\frac{(T_{\mathrm{SET}}-T_{\mathrm{M}})}{2}\right)\phi\right] \tag{20}$$

Substituting the scale of τ from Eq. (20) into Eq. (18) and using a Stefan Number and thermal capacity ratio defined respectively as,

$$Ste=\frac{c_{\mathrm{PCM}}(T_{\mathrm{SET}}-T_{\mathrm{M}})}{L} \tag{21}$$

and

$$\gamma=\frac{(\rho c)_{\mathrm{BM}}}{(\rho c)_{\mathrm{PCM}}} \tag{22}$$

one can arrive at the scale for the best δ that completely melts the PCM domain of the ECHS when the SPT is reached for any ϕ, as

$$\delta_{\mathrm{c}}\sim\zeta\left[\frac{(1-\phi)^2}{\phi}\left(1+\frac{Ste}{2}+\gamma Ste\frac{1-\phi}{\phi}\right)\right]^{\frac{1}{2}} \tag{23}$$

where

$$\zeta=\left[\frac{A(T_{\mathrm{SET}}-T_{\mathrm{M}})k_{\mathrm{PCM}}}{q}\right]^{\frac{1}{2}} \tag{24}$$

can be viewed as a characteristic length scale of the system. Along with Eqs. (21) and (22), it is one of the design parameters for the ECHS. Eq. (23) asymptotically predicts $\delta_{\mathrm{c}}\to\infty$ when $\phi\to 0$, and $\delta_{\mathrm{c}}\to 0$ when $\phi=1$. It is worth recalling however at both the limits (i.e. $\phi=1$ and 0) the scaling results of Eqs. (18) and (23) are invalid as at these limits, the scaling in Eq. (15) itself is no longer valid.

In addition, when the sensible heat contribution of the melted PCM is neglected (last term in Eq. (7)), as $Ste=0$, δ_{c} in Eq. (23) will be under-predicted. Hence for same ϕ, the corresponding B_{c}, Eq. (18), will also decrease (as τ, Eq. (20), decreases) resulting in more number of fins (F) than is actually necessary, causing the PCM portions of the CHS to melt completely *before* the SPT is reached (at an earlier time).

8. Best δ versus ϕ

Using an equation similar to Eq. (23), for a chosen BM/PCM combination and range of A and q'' (Table 1), the numerical results for a fixed T_{SET} determining the δ_{c} for each ϕ are regressed as

$$\delta_{\mathrm{c}}\sim K\times\left[\zeta^2\frac{(1-\phi)^2}{\phi}\left(1+\frac{Ste}{2}+\gamma Ste\frac{1-\phi}{\phi}\right)\right]^{\frac{1}{2}} \tag{25}$$

where the factor K accounts for the differences between the numerical solution and the scaling estimate of Eq. (23). Fig. 6 displays the comparison of the δ_{best} prediction for each ϕ from scaling analysis, Eq. (23), and the curve-fit using Eq. (25) with the numerical simulation data for $A=0.05$ m, at two heat flux values, $q''=2$ kW/m^2 and 25 kW/m^2. To quantify the goodness of the fit a relative average deviation is defined as

$$\sigma_{\mathrm{REL}}=\left[\frac{1}{N}\sum_{1}^{N}\left(\frac{\delta_{\mathrm{Eq.\ (25)}}-\delta_{\mathrm{S}}}{\delta_{\mathrm{S}}}\right)^2\right]^{1/2} \tag{26}$$

where N is the sample size (8) for each data set and $\delta_{\mathrm{Eq.\,(25)}}$ and δ_{S} are the values calculated respectively using Eq. (25) and the numerical solutions. A relative average deviation is used in Eq. (26) since the δ_{c} values in Fig. 6 differ in orders of magnitude and Eq. (26) 'normalizes' the deviation. The predictions from Eq. (25) with $K=0.732$ (continuous curve in Fig. 6a and b) yield a σ_{REL} within 4% when compared with the

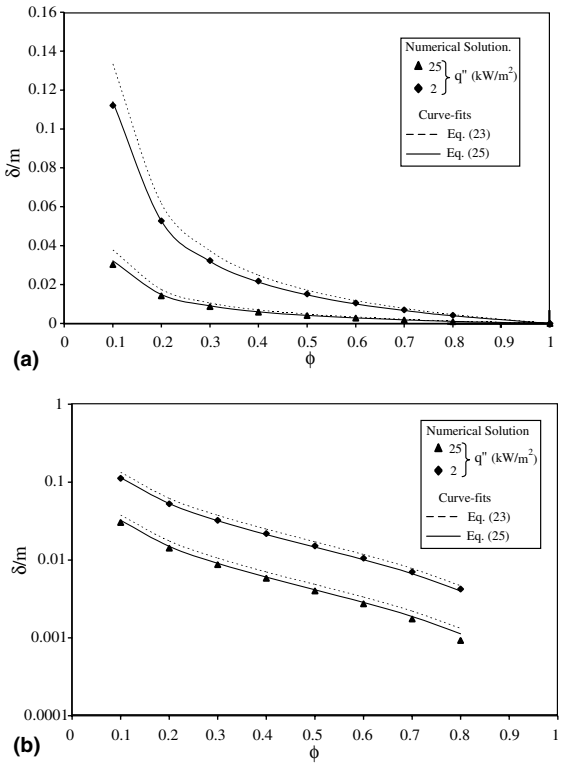

Fig. 6. (a) δ_{c} versus ϕ of the ECHS with $A=0.05$ for two heat fluxes and (b) semi-log plot of results in (a).

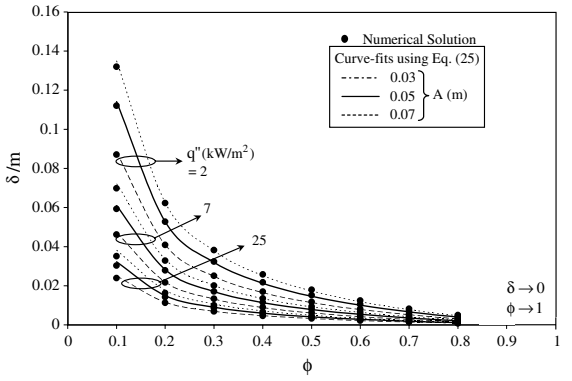

Fig. 7. Numerical solution results and predictions from scaling analysis for δ_c versus ϕ for the entire range of q'' and A (Table 1).

corresponding numerical data. The performance of the correlation Eq. (25) and the scaling estimate Eq. (23) in predicting the numerical data is better captured in the semi-log plot of Fig. 6b. The deviation of the predictions of Eq. (23) from the numerical data is almost systematic except when $\phi \to 1$ for large heat flux ($q = 25$ kW/m^2). The scaling estimate for δ_c, Eq. (23), obtained by assuming a linear temperature profile in the molten PCM and a lumped treatment of the BM domain, could fail for large heat fluxes. Neither numerical data nor estimates from Eqs. (23) and (25) are given at the limits (i.e. $\phi = 1$ and 0), for reasons stated earlier under Eq. (23), but the asymptotic limits for δ_c at these limits are displayed on the graph.

Fig. 7 displays all of the numerical data set for δ_c versus ϕ (for the entire range of A and q'' in Table 1) curve-fit using Eq. (25) with $K = 0.732$ itself and the fit is seen to be excellent yielding $\sigma_{REL} < 10\%$. The maximum deviation of the curve ($\sim$9%) from the data occurs for the data set with maximum values of q'', A and ϕ. Although a large A (see Fig. 1a and b) might encourage the linear temperature profile assumption in the PCM domain of the ECHS, it weakens the lumped BM assumption—which undermines the strength of Eq. (20) in predicting a correct scale for the time of operation. For larger values of q as well, as stated earlier, the linear temperature profile and lumped BM assumptions begin to fail.

9. The enhancement factor

For a given amount of PCM (ϕ), the enhancement factor, E_R, Eq. (9), could be rewritten as

$$E_R = \frac{E_{NI}(\phi)}{E_{NI}|_{\phi=0}} = \frac{q''(B+\delta)\tau_\phi}{q''(B+\delta)\tau_{\phi=0}} = \frac{\tau_\phi}{\tau_{\phi=0}} \qquad (27)$$

where, τ_ϕ is the time taken for an ECHS with finite PCM ($\phi \neq 0$) to reach the SPT and $\tau_{\phi=0}$ is the time taken to reach the SPT by an identical geometry of ECHS made only of BM ($\phi = 0$). Using Eq. (27), E_R, can be viewed as either the ratio of energy per unit area dissipated into the non-isothermal CHS to the energy per unit area dissipated into a non-isothermal CHS made only of BM ($\phi = 0$), *or* the ratio of the time of operation of the non-isothermal CHS (made of critical dimensioned ECHS) with the PCM and the non-isothermal CHS without the PCM ($\phi = 0$).

The best (maximum) values of τ_ϕ and $E_{NI}(\phi)$ can be obtained from numerical solutions as the time when SPT is reached and the corresponding energy stored in the domain—with ECHS dimensions at δ_c and B_c for each ϕ for the entire range of q and A tested. Plotted as symbols in Fig. 8 are the numerically generated data set of the E_R, Eq. (27), versus ϕ for the best values of either ϕ or $E_{NI}(\phi)$, for all of the range of q'' and A tested (Table 1). The values are seen to vary within 2% (error bar range in Fig. 8) of the average case, which is shown as the dark continuous curve-fit line. The region of space below this 'best' E_R values is represented by the performance of an identical non-isothermal CHS with improperly dimensioned ECHS.

The uppermost curve in Fig. 8 shows the performance of an ideal, *isothermal* CHS (storing maximum energy, Eq. (7)), where E_R is purely a function of ϕ alone and can be calculated using Eq. (9) with the numerator and denominator on the RHS obtained directly from Eq. (7) for any ϕ ($\neq 0$) and for $\phi = 0$ respectively. The difference in the isothermal and non-isothermal E_R is due to the temperature gradients present in the PCM domain of the ECHS (BM is highly conductive)—the reason why the difference between the curves grows as ϕ increases. The difference is the imprint of thermodynamic irreversibility in storing energy in a non-isothermal CHS.

Finally, the τ_ϕ in Eq. (27) can also be obtained directly using the scaling estimate for τ in Eq. (20), with

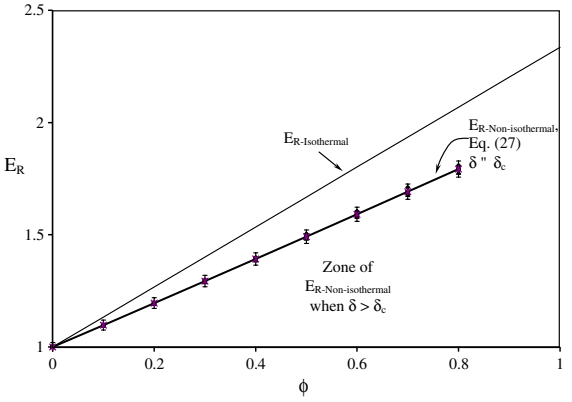

Fig. 8. Enhancement factor E_R versus ϕ for the entire range of q'' and A (Table 1).

a lumped BM and linear temperature profile in the molten-PCM assumptions. The linearity of the E_R versus ϕ for the numerical data-set in Fig. 8 shows these scaling assumptions are reasonable which is exemplified by the ratio

$$\Psi = \frac{\tau_\phi|_{\text{num}}}{\tau_\phi|_{\text{Eq. (20)}}} \tag{28}$$

when computed, yields a $\Psi \sim 1$ within 1% accuracy for all of the numerically simulated data-set in Fig. 8. To summarize, for operating under a given SPT (Eq. (1)) with a given amount of PCM (ϕ) and BM ($1-\phi$), the performance of a CHS constructed with the design in Fig. 1, can be improved for a given range of q'' and A (Table 1) by choosing the dimensions of the ECHS to be less than the critical dimensions ($\delta < \delta_c$ and $B < B_c$) with the help of Eqs. (25) and (10). Using Eq. (20), the E_R for such a non-isothermal CHS can be obtained from Eq. (27).

For an illustration of the method discussed in this paper, consider a cooling application that requires a thermal dissipation of 62.5 W and the electronics to be maintained below $T_{SET} = 90$ °C through a typical CHS area of 5 cm × 5 cm. For the above case then $q = 25$ kW/m^2 and by choosing a CHS with $D = 5$ cm and height $A = 5$ cm (Fig. 1), the number of critical dimensioned ECHS (Fig. 1b) made of 50% PCM (with $\phi = 0.5$) that should 'fill' the CHS (Fig. 1a) can be calculated using N, Eq. (11) once δ_c, Eq. (25) and B_c, Eq. (10) are determined. For this example ($\phi = 0.5$), since the value of $\delta_c = B_c = 0.004$ m, $N = 3.2$ and the time of operation of the CHS can be obtained from Eq. (20) as 425 s. If N is chosen as 4, the next integer, then the time of operation obtained numerically is 453 s. However, if for the same percentage of PCM ($\phi = 0.5$), N is chosen randomly as 3 or 2, then the ECHS becomes improperly dimensioned and the time of operation comes down dramatically to 410 and 294.5 s respectively (obtained from numerical solutions for the ECHS considered). On the other hand, if N is 9, the PCM fully melts well before the time at which SPT is reached. However, the increase in the time of operation of 456 s is marginal—a result of energy getting stored as sensible heat in the molten PCM.

10. Conclusions

For a CHS constructed with the design of BM fins placed vertically inside a PCM bath (Fig. 1a), operating under a given temperature set-point criterion (i.e. keeping the electronics that need to be cooled), under-usage of the latent heat of the PCM because of incomplete melting is a more critical CHS issue than the complete melting of PCM before the CHS reaches the SPT. The former results in a poorly performing CHS while the latter merely reduces the CHS potency for heat transfer enhancement (from PCM latent heat to sensible heat) in time.

Using simple scale analysis, the novel thermal design procedure enumerated in this paper solves the above issue by determining for a chosen ϕ, a "critical upper-bound dimension" (δ_c and B_c) for the ECHS. Constructing a CHS with ECHS made of the critical dimensions ($\delta = \delta_c$ and $B = B_c$) ensures complete melting of *all* of the PCM *exactly when* the SPT is reached. While the case where the ECHS dimensions are $\delta < \delta_c$ and $B < B_c$ also completely melts all of the PCM *before* the SPT is reached, its heat transfer enhancement potency reduces (to sensible heat) and because of more number of ECHS fins, may be unsuitable for manufacturing in certain configurations.

In addition, numerical solutions are generated to validate and augment the scaling analysis predictions of the critical dimensions of the ECHS. A correlation is also proposed (Eq. (25)), which in combination with Eq. (10) can predict the critical dimensions of the ECHS within 10% average deviation. Using the critical dimensions for the ECHS results in the maximization of the energy stored and time of operation of the CHS, as shown in the enhancement factors (E_R) of Fig. 8, when the CHS is constrained to use only the latent heat storage of the PCM. This is also illustrated with a practical microprocessor cooling example in the final section. Finally, although the results and the proposed correlation, Eq. (25), are done for a given range of heat flux, q'', and height, A, of the CHS, the thermal design procedure for finding the ECHS critical dimensions detailed in this paper is valid for all CHS composed of high latent heat storage PCM and high conductive BM, provided it is constructed with the design in Fig. 1.

References

[1] J.C. Bass, D.T. Allen, S. Ghamaty, N.B. Elsner, New technology for thermoelectric cooling, in: 20th IEEE SEMI-THERM Symposium, 2004, pp. 18–20.
[2] E.M. Alawadhi, C.H. Amon, Thermal analyses of a PCM thermal control unit for portable electronic devices: experimental and numerical studies, in: 2002 Inter Society Conference on Thermal Phenomena, 2002, pp. 466–475.
[3] F.L. Tan, C.P. Tso, Cooling of mobile electronic devices using phase change materials, Appl. Thermal Eng. 24 (2004) 159–169.
[4] S. Krishnan, S.V. Garimella, Analysis of a phase change energy storage system for pulsed power dissipation, Proc. IEEE Trans. Compon. Packag. Technol. 27 (1) (2004) 191–199.
[5] V.V. Kulish, J.L. Lage, Diffusion within a porous medium with randomly distributed heat sinks, Int. J. Heat Mass Transfer 43 (2000) 3481–3496.

[6] J.L. Lage, A.K. Weinert, D.C. Price, R.M. Weber, Numerical study of a low permeability microporous heat sink for cooling phased-array radar systems, Int. J. Heat Mass Transfer 39 (1996) 3633–3647.
[7] L.C. Chow, J.K. Zhong, Thermal conductivity enhancement for phase change storage media, Int. Commun. Heat Mass Transfer 23 (1) (1996) 91–100.
[8] M.M. Farid, A.M. Khudhair, S.A.K. Razack, S. Al-Hallaj, A review on phase change energy storage, materials and applications, Energy Convers. Manage. 45 (2004) 1597–1615.
[9] P. Lamberg, K. Siren, Approximate analytical model for solidification in a finite PCM storage with internal fins, Appl. Math. Model. 27 (2003) 491–513.
[10] K. Sasaguchi, K. Kusano, Solid/liquid phase change heat transfer in porous media (Effects of Fins on the Solidification Process), Heat Transfer—Japanese Res. 22 (1993) 398–415.
[11] S. Krishnan, S.V. Garimella, S.S. Kang, A novel hybrid heat sink using phase change materials for transient thermal management of electronics, in: Proceedings of 2004 Inter Society Conference on Thermal Phenomena (ITHERM04), pp. 310–318.
[12] Z. Zhang, A. Bejan, Melting in an enclosure at constant rate, Int. J. Heat Mass Transfer 32 (6) (1990) 1063–1076.
[13] D. Pal, Y.K. Joshi, Melting in a side heated tall enclosure by a uniformly dissipating heat source, Int. J. Heat Mass Transfer 44 (2001) 375–387.
[14] C.Y. Zhao, T.J. Lu, Analysis of microchannel heat sinks for electronics cooling, Int. J. Heat Mass Transfer 45 (2002) 4857–4869.
[15] Z. Liu, C. Ma, Numerical analysis of melting with constant heat flux heating in a thermal energy storage system, Energy Convers. Manage. 43 (2002) 2521–2538.
[16] S.S. Shastri, R.M. Allen, Method of lines and enthalpy method for solving moving boundary problems, Int. Commun. Heat Mass Transfer 25 (4) (1998) 531–540.
[17] B. Binet, M. Lacroix, Etude numerique de la fusion dans des enceintes rectangularies chauffees uniformement ou discretement par les parois laterales conductrices, Rev. Gen. Therm. 37 (1998) 607–620.
[18] N. Shamsundar, E.M. Sparrow, Analysis of multidimensional conduction phase change via enthalpy model, ASME J. Heat Transfer 97 (1975) 333–340.
[19] P.J. Roache, Computational Fluid Dynamics, Hermosa, 1972, pp. 91–95.
[20] A. Bejan, Heat Transfer, John Wiley & Sons, Inc, New York, 1993.
[21] C.Y. Li, S.V. Garimella, J.E. Simpson, Fixed-grid front tracking algorithm for solidification problems: Part I: Method and validation, Num. Heat Transfer Part B 43 (2003) 117–141.
[22] A. Haji-Sheikh, J. Eftekhar, D. Lou, Properties of paraffin wax as a thermal storage medium, in: Proceedings of AIAA/ASME Joint Thermo-physics, Fluids, Plasma and Heat Transfer Conference, AIAA, June 1982.